ISSN (Print) 1226-1750
ISSN (Online) 2233-6656
Journal of Magnetics 30(4), 825-836 (2025) https://doi.org/10.4283/JMAG.2025.30.4.825

Verifying the Reliability of a Hardware-Implemented TIS System in Phantom and Ex-vivo Experiments

Nayun Seo[1†], Seungmin Hwang[2†], Taegyu Kim[2], Yeonghun Song[1], Doyoung Pyeon[2], Youngjin Jung[3]*, and Jangwoo Park[1,3]*

[1]Korea Radioisotope Center for Pharmaceuticals, Korea Institute of Radiological & Medical Sciences, Nowon 01812, Republic of Korea
[2]Department of Biomedical Engineering, Chonnam National University, Yeosu 59626, Republic of Korea
[3]School of Biomedical Engineering, Chonnam National University, Yeosu 59626, Republic of Korea

(Received 6 November 2025, Received in final form 24 December 2025, Accepted 24 December 2025)

Temporal Interference Stimulation (TIS) advancement is hindered by technical limitations. This study aims to overcome these by developing a precision system and experimentally validating its core principle, focal point steering via current ratio control, through cross-validation in phantom, ex vivo, and computational models. We performed invasive experiments applying 108 and 100 Hz for an 8 Hz difference at 1:1, 2:1, and 1:2 ratios, maintaining 2.1 mA total current, in phantoms, ex vivo mouse brain, and muscle. Results consistently matched TIS theory: the 8 Hz envelope peak was centered at 1:1 and predictably shifted toward the weaker current side at 2:1/1:2 ratios. High concordance between experiments and simulations confirmed steering was maintained despite different tissue impedances. This integrative validation confirms TIS steering feasibility and provides a validated platform for future personalized stimulation.

Keywords : temporal interference stimulation, TIS Hardware, ex-vivo experiment, simulation

1. Introduction

Non-Invasive Brain Stimulation (NIBS) is a technology based on the principle of modulating neuronal activity and inducing neuroplasticity by applying magnetic or electric fields to the brain through the scalp [1]. Previous studies have demonstrated the clinical efficacy of conventional NIBS; for instance, transcranial Direct Current Stimulation (tDCS) has been shown to significantly improve upper-limb functions, such as hand grip strength and manual dexterity, by targeting the primary motor cortex (M1) in chronic stroke patients [2]. However, conventional NIBS methods such as transcranial Direct Current Stimulation (tDCS) and transcranial Alternating Current Stimulation (tACS) have a fundamental physical limitation. As the electric field passes through the skull and soft tissues, it undergoes significant attenuation, causing the stimulation to be concentrated primarily in the superficial cortex and making it difficult to deliver a sufficiently strong stimulus to deep brain structures [3-5]. Furthermore, their low spatial focality can lead to the stimulation of non-target areas, such as the scalp and facial muscles, which has been reported to cause sensory side effects [6, 7].

To overcome these limitations, Temporal Interference Stimulation (TIS) has been proposed [8]. TIS is based on the principle of applying two high-frequency currents (e.g., 2,000 Hz and 2,010 Hz) to the scalp, which generates a low-frequency envelope at the difference frequency (Δf) only in the deep target region where the currents overlap [9]. The high-frequency carriers themselves (in the kHz range) are above the response range of the neural membrane, resulting in relatively low neuronal recruitment along their paths. The low-frequency component is thereby emphasized at the location of the envelope, giving TIS the potential to maximize its effect on a deep target while minimizing direct stimulation of the overlying cortex [10]. The most innovative aspect of TIS is the ability to non-invasively steer the location of this envelope—the point of maximal stimulation—by adjusting

*Corresponding author: Tel: +82-2-970-8927
e-mail: jangwoo@kirams.re.kr
Tel:+82-61-659-7366, e-mail: yj@jnu.ac.kr
†These authors contributed equally to this work

the intensity ratio of the currents applied to the two electrode pairs [8]. This is critically important, as different neurological and psychiatric disorders such as Parkinson's disease, epilepsy, and depression are associated with dysfunction in different deep brain structures or circuits. This steering function is a key feature that could fundamentally solve the problem of low spatial focality in conventional neuromodulation and opens the possibility for patient-specific precision therapies that accurately target the pathological source of a disease [11].

The principles of TIS have been progressively validated in various studies beyond theory. The seminal study by Grossman *et al.* successfully induced selective motor responses in different body parts of living mice by modulating the current ratio [8], while Botzanowski *et al.* demonstrated therapeutic potential by suppressing disease biomarkers in a mouse model of epilepsy [12]. However, despite this innovative potential, the advancement of TIS research faces a significant technological bottleneck: the lack of commercially available, dedicated stimulators. Pioneering studies, such as those by Grossman *et al.* and Acerbo *et al*., had to rely on makeshift approaches, such as synchronizing two independent function generators [8, 10]. This configuration has clear limitations, as it is prone to phase drift between the two channels, which compromises the stability and reproducibility of the stimulation. This absence of reliable hardware acts as a key bottleneck, slowing down subsequent research aimed at validating the principles of TIS and exploring its clinical applications.

This study aims to experimentally validate the principle of stimulation location shifting through current ratio control and to develop a precision stimulation system that overcomes the technical limitations of TIS. It also aims to verify the reliability and accuracy of the system through cross-validation among phantom, ex vivo, and computational simulation models. Ultimately, the study aims to establish the physical validity of TIS and demonstrate its potential for personalized stimulation and clinical application expansion.

2. Methods

2.1. Development of the TI Stimulator

The developed system synchronously drives two or more pairs of independent current sources to precisely control their phase and amplitude. To circumvent the issue of fixed potentials, which arises from sharing a common reference between channels, we adopted a bipolar current source architecture. In this design, each electrode is directly connected to either a current source or a current sink. This configuration prevents the electrode pairs from being locked at the same potential, thereby ensuring the intended summation of current densities and the formation of the temporal interference envelope at the target location.

Within the current source circuit, a 100 μA constant current flows from the P1 node through the variable resistor NR. This establishes a voltage at node V_{nr}, which is defined by the equation:

$$V_{nr}=V_{p1}+(100\ \mu A\times NR) \tag{1}$$

An operational amplifier (OPAMP) and a MOSFET form a feedback loop, which drives the voltage across a set resistor (R_{set}) to match V_{nr}. This generates a current, I_{set}, according to the formula:

$$I_{set}=(V_{nr}-V_{p1})/R_{set}=(V_{p1}+100\ \mu A\times NR-V_{p1})/R_{set}$$
$$=100\ \mu A\times(NR/R_{set}) \tag{2}$$

Consequently, the P2 node operates as a current sink (I_{sink}), drawing a total current of:

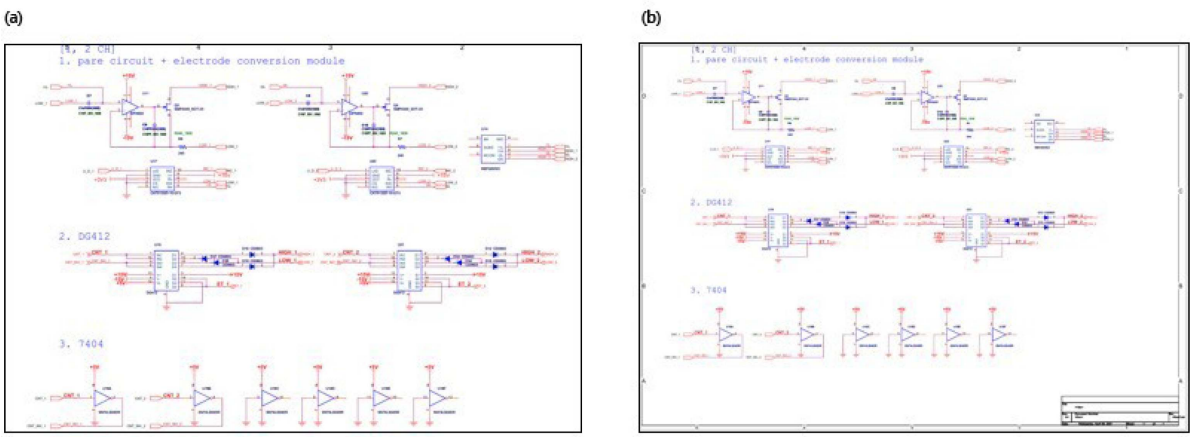

Fig. 1. (Color online) (a) Current Circuit, (b) Current Source, Sink, Analog Switch circuit.

$$I_{sink} = 100\ \mu A + I_{set} = 100\ \mu A + 100\ \mu A \times (NR/R_{set}) = 100\ \mu A(1+NR/R_{set}) \quad (3)$$

Conversely, the P1 node serves as the output, acting as a current source (I_{source}) with the same magnitude:

$$I_{source} = 100\ \mu A(1+NR/R_{set}) \quad (4)$$

Two such circuits were implemented to create a complete stimulation channel. The first circuit (Fig. 1a) was configured as a current source, with its P1 node connected to the voltage supply and its P2 node serving as the output. The second circuit (Fig. 1b) was configured as a current sink, with its P2 node connected to ground (GND) and its P1 node serving as the sinking terminal. With R_{set} fixed at 1 kΩ, the variable resistor NR was adjusted over a range of 0 to 19 kΩ, allowing the output current (I_{source} and I_{sink}) to be tuned from approximately 0.1 mA (minimum) to 2.0 mA (maximum), according to Eq. (4).

To generate the AC waveforms, analog switches were placed between the current sources and the electrodes, enabling the reversal of current direction. A sinusoidal waveform was generated by dynamically controlling the resistance of NR based on calculated sine values. The polarity of the output was determined by the sign of the sine function: a positive value corresponded to a forward current direction, while a negative value triggered the analog switches to reverse the current direction.

Based on this hardware capability, the operational current range and experimental current settings used in this study are summarized as follows. The stimulator supports an output current range of 0.1–2.0 mA per channel; however, for stable operation, the effective operational range was optimized to 0.5–1.5 mA, with a maximum load resistance of 5 kΩ. For all phantom and simulation experiments, the total summed current across the two stimulation channels ($I_{total} = I_1 + I_2$) was fixed at 2.1 mA. To implement specific current ratios while maintaining a constant I_{total}, the individual channel currents were set to 1.05 mA per channel for the 1:1 ratio, and to 1.4 mA and 0.7 mA for the 2:1 and 1:2 ratios, respectively.

2.2. Agar Phantom Fabrication and Electrode Configuration

The agar phantom used in the experiments was fabricated based on the study by D. Bennett *et al.* [13]. To mimic the electrical properties of biological tissue, the conductivity of the phantom was controlled by adjusting the concentration of sodium chloride (NaCl). The phantom was prepared in a plastic mold with dimensions of 10 cm (width) × 10 cm (length) × 3 cm (height).

For electrical stimulation and measurement, needle electrodes (DB106, DONGBANG MEDICAL, Seongnam-si, Gyeonggi-do, Republic of Korea) with a diameter of 0.16 mm and a length of 15 mm were used. The entire surface of each electrode, except for the 2 mm tip, was insulated using a liquid insulating compound (4228-55ML, MG Chemicals, Burlington, Ontario, Canada). A detailed image of the fabricated phantom is provided in Appendix B.

2.3. Equipment Setup

The TIS stimulator was wirelessly connected to a host computer via Bluetooth. The stimulation current and

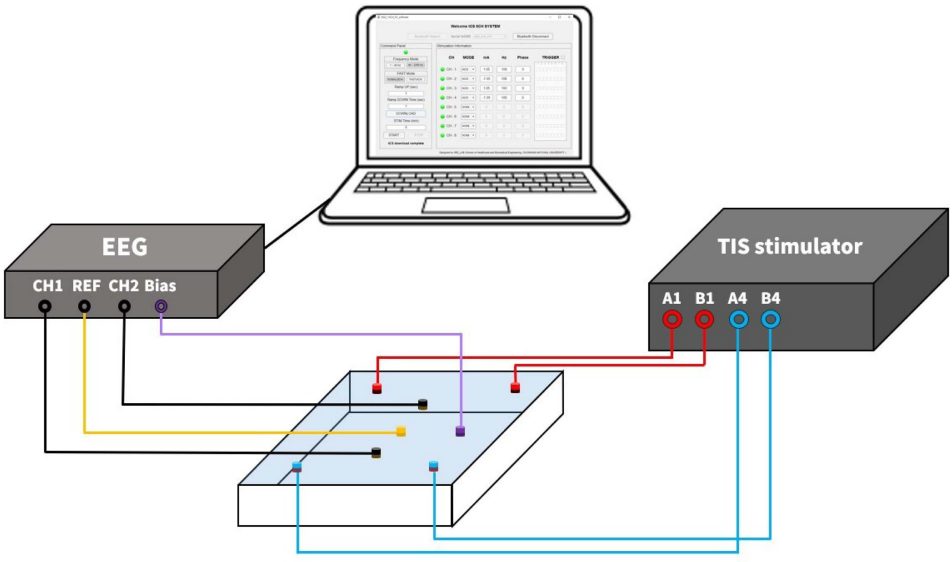

Fig. 2. (Color online) Experimental setup.

frequency were configured using a custom control program developed with MATLAB App Designer (2023b, MathWorks, Natick, MA, USA). The EEG device was connected to the host computer through a USB Type-C interface. Signal acquisition and storage were managed by a separate recording program, also developed using App Designer.

The overall experimental setup is illustrated in Fig. 2, and detailed figures are provided in Appendix A. Both the phantom and the ex-vivo experiments were conducted using identical stimulation and measurement parameters and the same electrode configuration. The only variable was the experimental subject (i.e., the agar phantom, mouse brain, or mouse muscle).

2.4. Animals

Male C57BL/6 mice (9 weeks old, n=2) were purchased from JA BIO (Suwon, Republic of Korea). Environmental conditions were maintained at a temperature of 25 ± 2 °C under a 12-h light/dark cycle. To reduce pain and stress potentially induced by invasive procedures such as electrode insertion, all measurements were carried out immediately following humane euthanasia. Animals were euthanized by CO_2 inhalation immediately prior to data acquisition. All animal experiments were conducted in compliance with the institutional guidelines of the Korea Institute of Radiology and Medical Sciences (KIRAMS) and were approved by the Institutional Animal Care and Use Committee (IACUC; approval No. KIRAMS 2025–0065).

2.5. Phantom Experiment

The phantom experiment was conducted by inserting stimulation electrodes at opposite ends of the phantom, as shown in Fig. 3a. In the center of the phantom, measurement electrodes (CH1, REF, CH2) were placed at regular intervals. All electrodes were inserted to a uniform depth of 7 mm. The stimulation protocol involved the simultaneous application of two different frequencies, f1 and f2, to two electrode pairs (A1-B1 and A2-B2). An 8 Hz difference frequency (Δf) was generated by applying a 108 Hz signal to the A1-B1 pair and a 100 Hz signal to the A2-B2 pair. The stimulation protocol consisted of a block design with three repetitions of a 10-second stimulation period followed by a 10-second rest period. Data were recorded for a total duration of one minute.

To observe the shift in the optimal stimulation, focus according to the current ratio, the phantom experiment was conducted under three current ratio conditions (1:1, 2:1, and 1:2). Stimulation was applied using the pre-

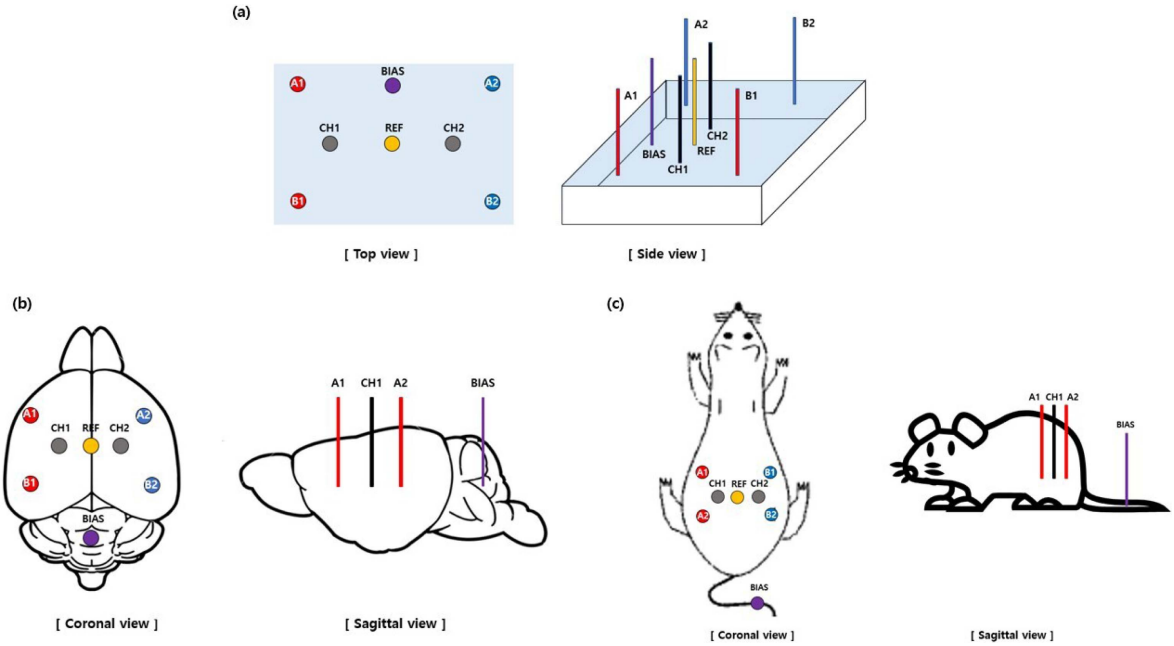

Fig. 3. (Color online) Electrode setup for phantom and ex-vivo experiments. (a) Schematic for the phantom experiment. (b) and (c) Schematics for the ex-vivo experiments on the mouse brain and thigh muscle, respectively. In all figures, A1-B1 (I_1) and A2-B2 (I_2) represent the stimulation electrode pairs, while CH1, REF, and CH2 denote the measurement electrodes. During stimulation, the current ratio (I_1:I_2) was adjusted while the total current sum (I_{total}=I_1+I_2) was kept constant. The BIAS electrode (purple) was positioned between A1 and A2 in the phantom experiment (a), on the cerebellum in the brain experiment (b), and on the tail in the muscle experiment (c). For detailed figures, refer to Appendix B and C.

defined current settings described in Section 2.1, while maintaining a constant total current (I_{total} = 2.1 mA) across all conditions. Biphasic currents were symmetrically delivered to each electrode pair, with carrier frequencies of 108 Hz and 100 Hz assigned to the A1–B1 and A2–B2 pairs, respectively.

2.6. Ex-Vivo Experiment

The ex-vivo experiments were performed using the same stimulation protocol as the phantom experiments described in Section 2.5. The experiments were conducted on two sites: the mouse brain and muscle, with needle electrodes inserted for both electrical stimulation and electric field measurement.

For the brain experiment, the skull was opened immediately after euthanasia to expose the brain tissue. One pair of electrodes (A1-B1 and A2-B2) was inserted into the left and right cerebral hemispheres, respectively. The REF and CH electrodes for EEG measurement were inserted as depicted in Fig. 3b. The needle electrodes were inserted to a depth of 6 mm into the brain tissue. For the muscle experiment, conducted as shown in Fig. 3c, the skin was removed immediately after euthanasia to verify that TIS generates an effective electric field within the muscle tissue. One pair of electrodes (A1-B1 and A2-B2) was inserted into the left and right thighs to a depth of 4 mm. Detailed figures are provided in Appendix B and C.

2.7. Signal Measurement and Analysis

The biopotential measurement device (EEG) used in the experiment was designed based on the reference circuit of the ADS1299, a multi-channel biopotential measurement IC. To ensure high input impedance and minimize drift and offset, the device incorporates differential inputs and a BIAS drive. For a stable power supply, Low-Dropout (LDO) regulators with noise levels below 100 μV (e.g., TPS7A25, TPS7A2033, Texas Instruments) were used. Data was acquired via a C2000 MCU (F28027) from Texas Instruments, which measured and recorded the potential difference between the CH and REF electrodes.

The acquired raw data were saved as .mat files and analyzed using MATLAB 2023b (MathWorks, Natick, MA, USA). The envelope was extracted by demodulating the difference frequency component ($\Delta f = |f_2 - f_1|$), which is the key component of TIS. A 1 Hz high-pass filter was subsequently applied to remove noise. The final envelope amplitude was defined as the difference between the local maximum of the upper envelope and the local minimum of the lower envelope within a single Δf cycle.

The electric field (V/mm) was calculated by dividing the measured potential difference between each CH electrode and the REF electrode by the fixed inter-electrode distance. The REF electrode served as a local reference point to minimize common-mode interference. Identical electrode geometry and spacing were applied across phantom, ex vivo, and simulation conditions to ensure comparability.

2.8. Simulation Methodology and Setup

The TIS simulation in this study was performed using NEO, a platform for simulating and analyzing non-

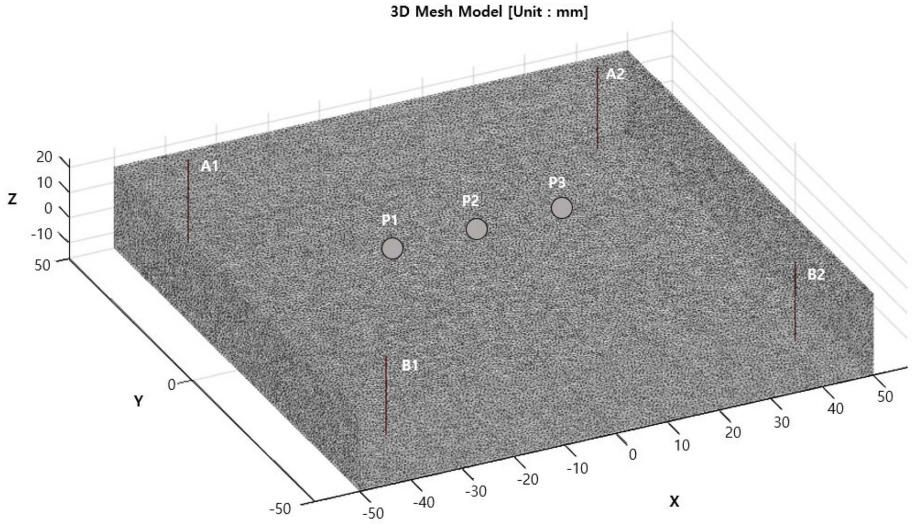

Fig. 4. The 3D mesh simulation model of the phantom. Only the conductive medium of the phantom is displayed. The four needle electrodes were configured into two stimulation pairs (A1-B1, A2-B2). The observation points P1-P2-P3 correspond to the CH1-REF-CH2 locations in the actual experiment, and the envelope metric is calculated at each of these points. The simulated phantom model was set to the same dimensions as the actual phantom: 100 mm in width, 100 mm in length, and 30 mm in height.

invasive brain stimulation. First, a cube model with the same size and shape as the agar phantom was created using Iso2Mesh [14]. Next, needle electrodes of the same dimensions as those used in the actual experiment were modeled and inserted at identical locations, resulting in a simulation model with a total of four electrodes. The node and element information for the simulation model is as follows: 364,121 nodes × 3 and 2,085,633 elements × 4. The conductivity of the simulated phantom was set to 0.22 S/m.

The simulation was run by inputting the conductivity [S/m], frequency [Hz], and current [A] for each needle electrode and the cube model. From the simulation results, points corresponding to the coordinates of the EEG electrodes were selected, and the TIS interference waveform over a 0–1 second interval was extracted. The resulting modulated waveform from this interference pattern was then analyzed. The setup for the comparative simulation of the phantom experiment is depicted in Fig. 4.

3. Results

3.1. TIS Device Development Results

The system was designed in three parts—a power supply unit, a control unit, and a stimulation unit—which were integrated onto a single PCB. The power supply unit provides separate rails for the OPAMPs and switches. The control unit sets the level and direction of the output current by adjusting variable resistors and analog switches. The stimulation unit outputs the source/sink current for each channel according to the resistance of the input variable resistor. The PCB artwork (Fig. 5a) minimized inter-channel leakage and parasitic coupling by incorporating zone separation for each function, symmetric routing, and careful layout of high-impedance sections. The completed device enclosure was designed for user-friendly maintenance, featuring CH1–CH8 output terminals and status LEDs (ON/BAT/STIM) and the main power switch on the front panel, with a battery charging port on the rear panel (Fig. 5b).

The key specifications of the transcranial current stimulation (tCS) system developed in this study are as follows. The output current is adjustable within a range of 0.5–1.5 mA, with a maximum load resistance of 5 kΩ. A ramp-up/ramp-down feature was implemented to ensure the current gradually reaches the target intensity at the onset and conclusion of stimulation, facilitating a smooth process.

The stimulation frequency is configurable from 1 to 2250 Hz, with a high-speed tACS mode that extends the operational frequency up to 4500 Hz. Additionally, the system supports both internal and external trigger functions. The internal trigger is designed for automated operation, initiating and terminating stimulation across 8 channels based on a pre-set sequence and range, with a trigger step time of 10 μs. The external trigger is configured as a safety measure, designed to immediately terminate stimulation upon the detection of a HIGH signal at any of the eight input terminals.

3.2. Phantom Experiment Results

Figures 6a, 6b, and 6c show the potential difference signals and corresponding envelope graphs measured by the EEG under different current ratios during TI stimulation of the phantom. The experimental results confirmed that at the location of optimal stimulation, the depth of the envelope (the red curve in the graph) increased, corresponding to a larger amplitude. At a 1:1 current ratio (Fig. 6a), the envelope amplitude of the

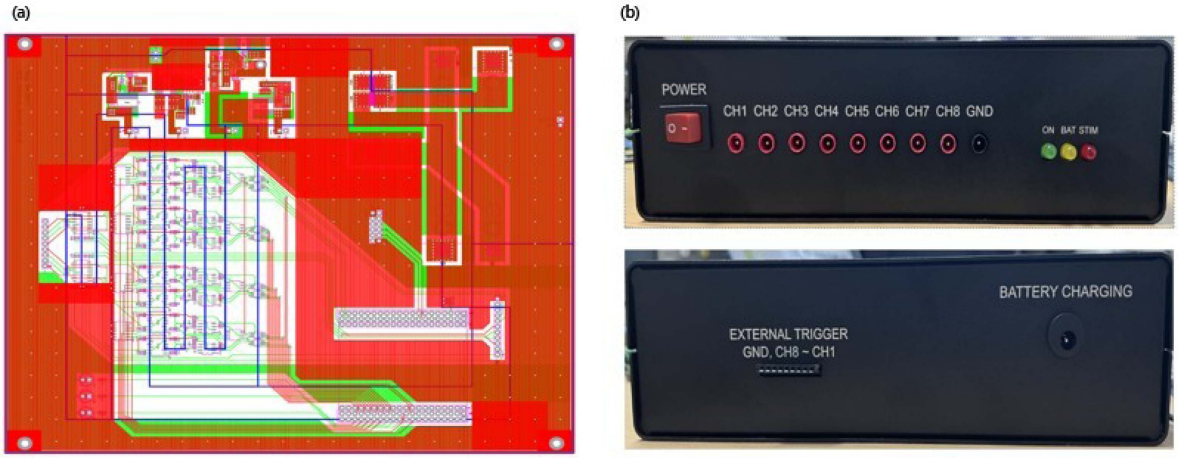

Fig. 5. (Color online) (a) Design Artwork of the TIS device, (b) Assembly of the TIS device.

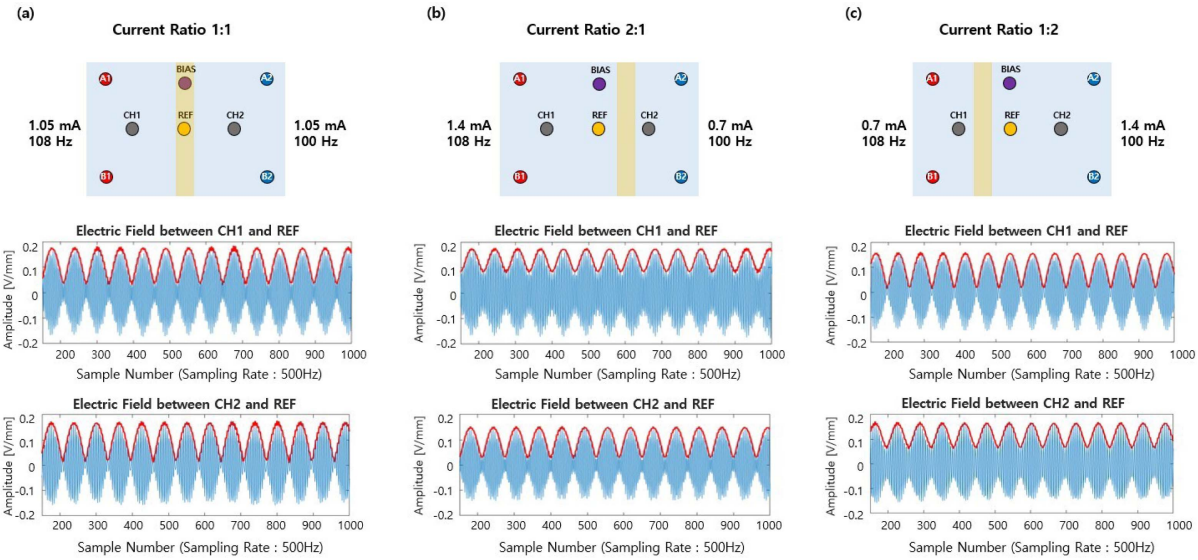

Fig. 6. (Color online) Phantom experiment results under different current ratio conditions. Panels (a–c) correspond to the 1:1, 2:1, and 1:2 current ratios, respectively. The upper schematics illustrate the stimulation and measurement electrode configuration, with yellow bars indicating the theoretically predicted optimal stimulation focus. The lower plots show the measured electric fields and corresponding envelopes (red curves). As the current ratio changes, the envelope peak shifts spatially from the center (1:1) toward the right (2:1) or left (1:2), consistent with theoretical predictions.

signal measured between CH1-REF (left) was 0.124 V/mm, and the amplitude measured between CH2-REF (right) was 0.126 V/mm, indicating similar amplitudes on both sides. At a 2:1 current ratio (Fig. 6b), the envelope amplitude was 0.077 V/mm for CH1-REF (left) and 0.111 V/mm for CH2-REF (right), showing a larger amplitude on the right side. At a 1:2 current ratio (Fig. 6c), the envelope amplitude was 0.124 V/mm for CH1-REF (left) and 0.077 V/mm for CH2-REF (right), indicating a larger amplitude on the left side.

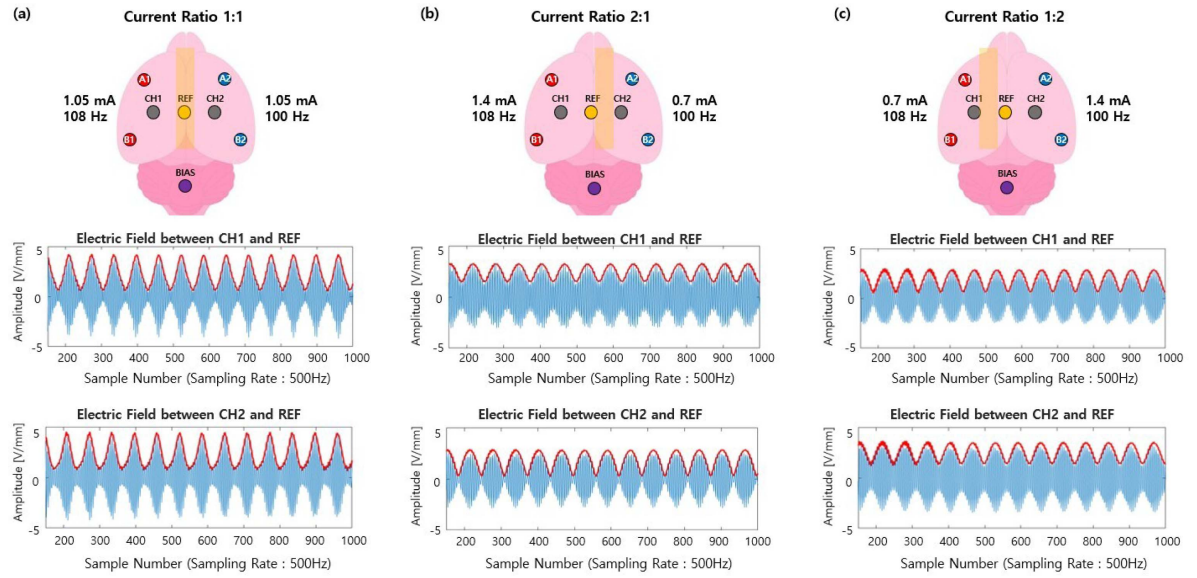

Fig. 7. (Color online) Mouse brain experiment results under different current ratio conditions. Panels (a–c) correspond to the 1:1, 2:1, and 1:2 current ratios, respectively. The upper schematics illustrate the stimulation and measurement electrode configuration, with yellow bars indicating the theoretically predicted optimal stimulation focus. The lower plots show the measured electric fields and corresponding envelopes (red curves). As the current ratio changes, the envelope peak is centered under the 1:1 condition and shifts toward the right (2:1) or left (1:2), consistent with theoretical predictions.

3.3. Ex-Vivo Experiment Results

Figures 7a, 7b, and 7c show the potential difference signals and corresponding envelope graphs measured by the EEG from the excised mouse brain under different current ratios. At a 1:1 current ratio (Fig. 7a), the envelope amplitude of the signal measured between CH1-REF (left) was 3.942 V/mm, and the amplitude measured between CH2-REF (right) was 3.828 V/mm, indicating similar amplitudes on both sides. In contrast, when the current ratio was changed to 2:1 (Fig. 7b), the amplitude at CH2-REF (right) (2.189 V/mm) was larger than at CH1-REF (left, 1.748 V/mm). Conversely, at a 1:2 ratio (Fig. 7c), the amplitude at CH1-REF (left) (2.152 V/mm) was dominant over that at CH2-REF (right, 1.709 V/mm). The experimental results confirmed that at the location of optimal stimulation, the depth of the envelope (the red curve in the graph) increased, corresponding to a larger amplitude.

Figures 8a, 8b, and 8c show the potential difference signals and corresponding envelope graphs measured by the EEG from the mouse thigh muscle under different current ratios. The envelope amplitudes measured under each current ratio condition were as follows (Fig. 8): at a 1:1 ratio, the values for CH1-REF (left) and CH2-REF (right) were similar (3.607 V/mm and 3.549 V/mm, respectively); at a 2:1 ratio, the amplitude at CH2-REF (right) was dominant (4.248 V/mm vs. 2.465 V/mm for CH1-REF); and at a 1:2 ratio, the amplitude at CH1-REF (left) was dominant (4.414 V/mm vs. 2.284 V/mm for CH2-REF). The experimental results confirmed that the envelope's depth (the red curve in the graph) and its corresponding amplitude increased at the location of optimal stimulation, which shifted according to the current ratio.

3.4. Simulation Results

Figures 9a, 9b, and 9c show the results derived from the phantom simulation under different current ratios during TI stimulation. At a 1:1 current ratio (Fig. 9a), the envelope amplitude of the signal between P1-P2 (left) was 0.218 V/mm, and between P2-P3 (right) was 0.233 V/mm, indicating similar amplitudes on both sides. At a 2:1 current ratio (Fig. 9b), the envelope amplitude was 0.145 V/mm for P1-P2 (left) and 0.281 V/mm for P2-P3 (right), showing a larger amplitude on the right side. At a 1:2 current ratio (Fig. 9c), the envelope amplitude was 0.269 V/mm for P1-P2 (left) and 0.156 V/mm for P2-P3 (right), indicating a larger amplitude on the left side. The results demonstrated that as the current ratio was adjusted, the red-colored region in the simulation image shifted, and the envelope amplitude increased at the location of optimal stimulation.

Figures 10a, 10b, and 10c show the results derived from the brain simulation under different current ratios during TI stimulation. Under the 1:1 current ratio condition (Fig. 10a), the envelope amplitudes for P1-P2 (left) and P2-P3

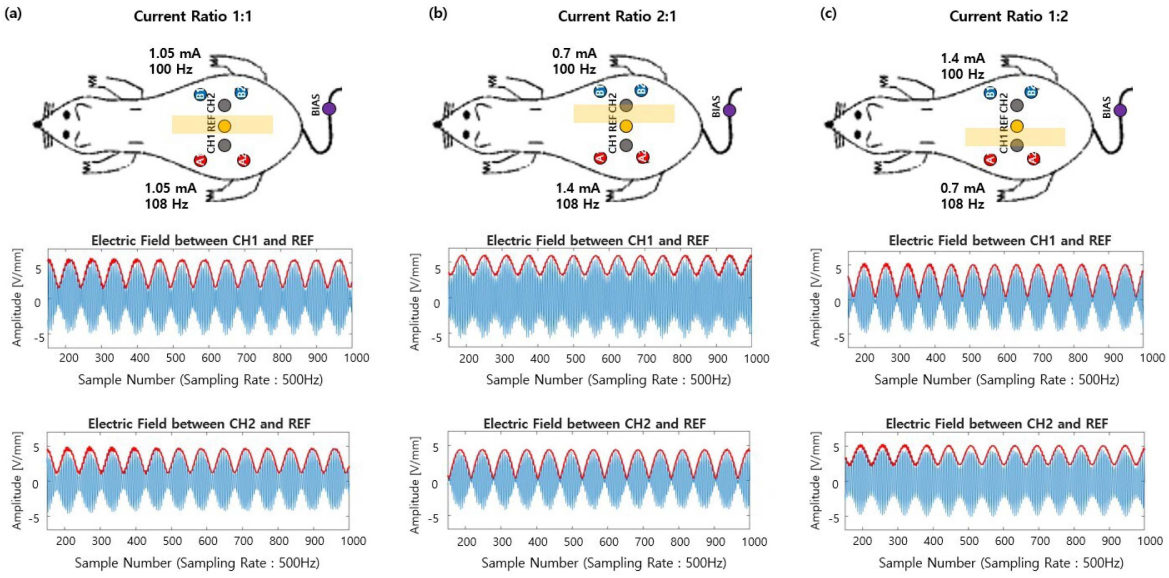

Fig. 8. (Color online) Mouse thigh muscle experiment results under different current ratio conditions. Panels (a–c) correspond to the 1:1, 2:1, and 1:2 current ratios, respectively. The upper schematics illustrate the stimulation and measurement electrode configuration, with yellow bars indicating the theoretically predicted optimal stimulation focus. The lower plots show the measured electric fields and corresponding envelopes (red curves). As the current ratio changes, the envelope peak is centered under the 1:1 condition and shifts toward the right (2:1) or left (1:2), consistent with theoretical predictions.

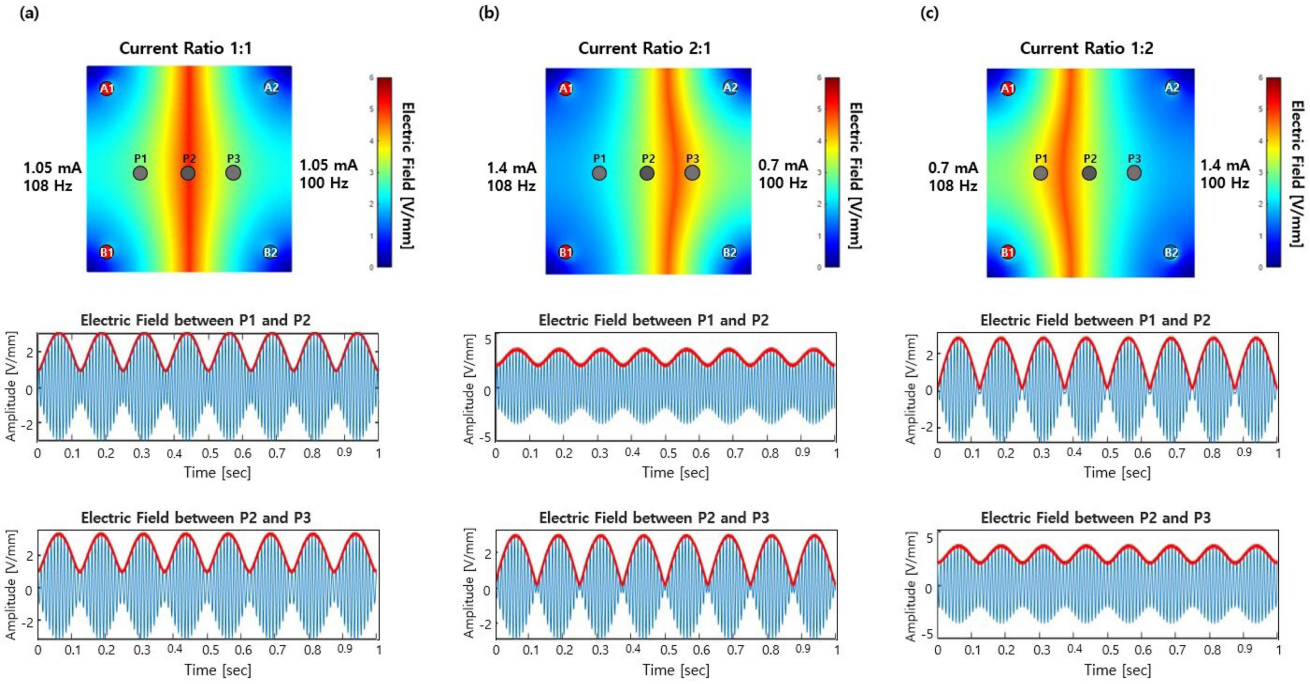

Fig. 9. (Color online) Phantom simulation results under different current ratio conditions. Panels (a–c) correspond to the 1:1, 2:1, and 1:2 current ratios, respectively. The upper panels show the simulated electric field distribution, with warmer colors indicating higher field intensity and proximity to the stimulation focus. The lower plots present the corresponding envelopes evaluated at P1–P2 and P2–P3. As the current ratio changes, the focal peak is centered in the 1:1 condition and shifts toward P3 in the 2:1 condition and toward P1 in the 1:2 condition, consistent with current-ratio–based steering.

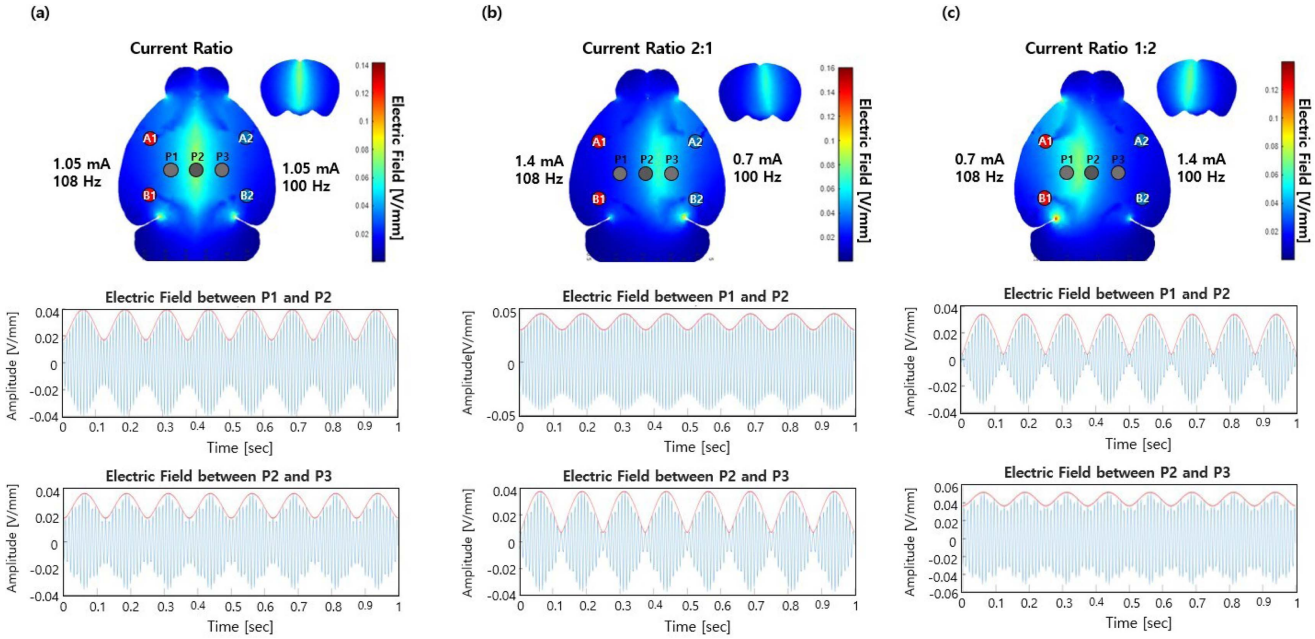

Fig. 10. (Color online) Mouse brain simulation results under different current ratio conditions. Panels (a–c) correspond to the 1:1, 2:1, and 1:2 current ratios, respectively. The upper panels display the simulated electric field distribution, with warmer colors indicating higher field intensity and proximity to the stimulation focus. The lower plots show the corresponding envelopes evaluated at P1–P2 and P2–P3. As the current ratio changes, the focal peak is centered in the 1:1 condition and shifts toward P3 in the 2:1 condition and toward P1 in the 1:2 condition, consistent with current-ratio–based steering.

(right) were identical at 0.023 V/mm. When the current ratio was changed to 2:1 (Fig. 10b), the amplitude at P2-P3 (right) (0.030 V/mm) was twice as large as that at P1-P2 (left, 0.015 V/mm). Conversely, at a 1:2 ratio (Fig. 10c), the amplitude at P1-P2 (left) (0.030 V/mm) was twice as large as that at P2-P3 (right, 0.015 V/mm). The results showed that as the current ratio was adjusted, the light-blue-colored region in the brain simulation image shifted, and the envelope amplitude increased at the location of optimal stimulation.

4. Discussion

This study integratively validated the physical principles and applicability of Temporal Interference Stimulation (TIS) through experiments and simulations, presenting new directions for TIS development and its potential for personalized stimulation. Key achievements include: first, demonstrating the feasibility of selective stimulation by experimentally confirming the focal point steering predicted by TIS theory. Second, confirming that TIS stimulation modulation amplitude varies systematically with impedance differences in conditions with distinct impedances (phantom, brain, muscle), yet selective stimulation of the target region is maintained. Third, demonstrating high concordance between simulation results in the phantom and brain and experimental results, suggesting the potential for personalized TIS applications.

While conventional TIS implementations typically use kilohertz-range carrier frequencies to take advantage of the low-pass filtering properties of neural membranes, the present study employed a different experimental approach. Lower carrier frequencies of 100 and 108 Hz were chosen to enable direct and high-resolution measurement of the interference envelope using a custom-developed EEG system. This frequency choice was not intended to replicate the neurophysiological operating regime of kHz-TIS, but to allow clear observation of the interference envelope and its spatial changes with current ratio modulation under controlled experimental conditions.

We confirmed the potential for precise control of the stimulation focal point by observing that the low-frequency envelope of TIS shifts spatially according to adjustments in the current ratio. The focal point was centered when the current ratio was identical, but shifted toward the side with the weaker current at ratios of 2:1 or 1:2. Peng *et al.* theoretically proposed that the spatial selectivity of TIS could be steered by adjusting the current ratio between electrodes, thereby changing the overlapping area of the two electric fields [15]. Grossman *et al.* demonstrated via simulations in a cylindrical phantom that the location of the maximum stimulation point could be precisely controlled by adjusting the current ratio applied to the two electrode pairs [8]. Furthermore, Su *et al.* observed in retinal stimulation modeling experiments that the target electric field moved toward the side with the weaker current as the ratio was adjusted, proposing that this current-ratio-based control is attributed to the principle of electric field superposition [16]. As such, our experimental results align with these prior studies and strongly support the established physical principles of TIS.

When the same TIS protocol was applied to a homogeneous phantom and complex brain/muscle tissues, the spatial characteristics of the stimulation location were well-maintained, but the magnitude of the envelope differed according to the material's conductivity. Electrical conductivity is known as the most critical and sensitive parameter determining current flow ($J = \sigma E$) and electric field distribution within a Volume Conductor model [17]. Bolfe *et al.* showed that as the distance between electrodes increases, effective conductivity decreases, thus increasing the potential difference, and demonstrated that biological tissue behaves like a frequency-dependent ohmic conductor, to which Ohm's law can be applied [18]. Additionally, Damijan *et al.* reported that the permittivity and electrical conductivity of biological tissues play a key role in the application of electrical stimulation [19]. The head possesses an extremely electrically heterogeneous structure due to the CSF, GM, WM, and skull [20, 21]. Tissues like WM and muscle also exhibit anisotropic properties, where current flows relatively easily along the direction of fiber bundles (longitudinal) but is restricted by high resistance in the transverse direction [22]. However, Vorwerk *et al*. concluded that in the complex conductivity landscape of GM and WM, the stimulation location is almost unaffected, whereas the electric field strength is strongly influenced [23]. Indeed, our results showed that the envelope magnitude was larger in muscle tissue with higher impedance and anisotropic properties than in the phantom, indicating that electrode–tissue impedance variability across phantom, brain, and muscle conditions primarily influences the absolute magnitude of the measured envelope amplitude. However, it is important to note that the primary focus of this study was not the absolute reproducibility of envelope amplitude values across different tissue types, but rather the reproducibility of the spatial steering behavior induced by current ratio modulation. In this regard, despite impedance-related amplitude scaling, the relative spatial distribution of the envelope and the direction of stimulation steering were consistently preserved across all conditions, demonstrating

that impedance heterogeneity affects envelope gain rather than the reproducibility of the steering mechanism itself. This demonstrates that, in our TIS system, the spatial resolution of steering is fundamentally determined by electrode geometric factors such as inter-electrode distance and arrangement, while tissue conductivity distribution and anisotropy act as secondary factors that modulate electric field strength and envelope amplitude rather than spatial resolution.

The high accuracy of computer simulations in phantom and brain tissues confirmed the potential for personalized precision stimulation. The computer simulation results, which mimicked the physical phantom and brain tissue, showed that the steering trend of the optimal stimulation point according to the current ratio was consistent with actual experimental results, although some discrepancies in the envelope values were observed. Prior research by Pursiainen *et al.* argued that inaccurate calculations of electrode-tissue contact impedance could cause errors between actual measurements and simulation results [24]. Furthermore, a study by Tiruvadi *et al.* reported that such impedance mismatches could cause non-linear signal distortion, introducing additional errors in the final measurements [25]. In our actual experiments, the electrodes were insulated except for the 2 mm tip, whereas the simulation assumed the entire electrode was a conductor, which we infer contributed to this difference. Nonetheless, the high concordance between our experimental results and the simulations regarding the key TIS metric, stimulation location steering holds significant meaning as a core technological platform for the expansion and advancement of TIS research.

Despite these findings, this study has several limitations. First, while we validated TIS selective stimulation theory using EEG, the experiments were conducted in a low-frequency band due to the high-frequency (kHz) measurement limitations of our custom-developed small-animal EEG system. Therefore, biological validation remains a future task to determine if the stimulation steering control verified here can induce the intended neurophysiological effects (e.g., selective deep stimulation) in the actual TIS therapeutic environment. Second, by using phantoms and ex vivo biological tissues rather than an in vivo setting, we did not capture potential differences present in a true in vivo environment, such as blood flow or real-time physiological responses. Third, we adopted an invasive measurement method by inserting internal electrodes for the precise validation of TIS theory, which does not mimic the electric field attenuation or distribution changes that occur in a real-world clinical setting, where current must pass through the scalp and skull.

This study is the first to integratively validate that the core physical principles of TIS hold true not only in simple phantom models but also across complex biological tissues with different impedance characteristics and in computer simulation environments. This integrative validation simultaneously demonstrates the feasibility of selective stimulation and its technological scalability. Furthermore, the high concordance with simulations supports the potential for personalized stimulation. Therefore, this study holds significant value as it helps resolve technical bottlenecks in TIS technology and provides a core technological platform for precision stimulation.

Acknowledgments

This study was supported by a grant of the Korea Institute of Radiological and Medical Sciences (KIRAMS), funded by Ministry of Science and ICT (MSIT), Republic of Korea (No. 50539-2025). In addition, This research was supported by the Bio&Medical Technology Development Program of the National Research Foundation (NRF) funded by the Korean government (MSIT) (No. RS-2021-NR056450), and by the "Regional Innovation System & Education (RISE)" through the Gwangju RISE Center, funded by the Ministry of Education (MOE) and the Gwangju Metropolitan Government, Republic of Korea (2025-RISE-05-011).

References

[1] S. Y. Yoon, Geriatr. Rehabil. **14**, 73 (2024).
[2] Y. W. Choi and S. M. Nam, J. Magn. **25**, 396 (2020).
[3] M. Voroslakos, Y. Takeuchi, K. Brinyiczki, T. Zombori, A. Oliva, A. F. Ruiz, G. Kozak, Z. T. Kincses, B. Ivanyi, G. Buzsaki, and A. Berenyi, Nat. Commun. **9**, 483 (2018).
[4] Y. Huang, A. A. Liu, B. Lafon, D. Friedman, M. Dayan, X. Wang, M. Bikson, W. K. Doyle, O. Devinsky, and L. C. Parra, Elife. **6**, e18834 (2017).
[5] T. G. Kim, N. Y. Seo, Y. J. Jung, and J. W. Park, J. Magn. **29**, 467 (2024).
[6] A. Antal, I. Alekseichuk, M. Bikson, J. Brockmöller , A. R. Brunoni, R. Chen, L. G. Cohen, G. Dowthwaite, J. Ellrich, A. Flöel, F. Fregni, M. S. George, R. Hamilton, J. Haueisen, C. S. Herrmann, F. C. Hummel, J. P. Lefaucheur, D. Liebetanz, C. K. Loo, C. D. McCaig, C. Miniussiv, P. C. Miranda, V. Moliadze, M. A. Nitsche, R. Nowak, F. Padberg, A. Pascual-Leone, W. Poppendieck, A. Priori, S. Rossi, P. M. Rossini, J. Rothwell, M. A. Rueger, G. Ruffini, K. Schellhorn, H. R. Siebneral, Y. Ugawaan, A. Wexler, U. Ziemann, M. Hallett, and W. Paulus, Clin. Neurophysiol. **128**, 1774 (2017).

[7] C. Poreisz, K. Boros, A. Antal, and W. Paulus, Brain Res. Bull. **72**, 208 (2007).
[8] N. Grossman, D. Bono, N. Dedic, S. B. Kodandaramaiah, A. Rudenko. H. J. Suk, A. M. Cassara, E. Neufeld, N. Kuster, L. H. Tsai, A. P. Leone, and E. S. Boyden, Cell. **169**, 1029 (2017).
[9] W. Guo, Y. He, W. Zhang, Y. Sun, J. Wang, S. Liu, and D. Ming, Front. Neurosci. **17**, 1092539 (2023).
[10] E. Acerbo, A. Jegou, C. Luff, P. Dzialecka, B. Botzanowski, F. Missey, I. Ngom, S. Lagarde, F. Bartolomei, A. Cassara, E. Neufeld, V. Jirsa, R. Carron, N. Grossman, and A. Williamson, Front. Neurosci. **16**, 945221 (2022).
[11] Z. Zhu, L. Qin, D. Tang, Z. Qian, J. Zhuang, Y. Liu, Brain Sci. **15**, 317 (2025).
[12] B. Botzanowski, E. Acerbo, S. Lehmann, S. L. Kearsley, M. Steiner, E. Neufeld, F. Missey, L. Muller, V. Jirsa, B. D. Corneil, and A. Williamson, Bioelectron. Med. **11**, 7 (2025).
[13] D. Bennett, Mater. Sci. Eng. C. **31**, 494 (2011).
[14] Q. Fang and D. A. Boas, Proc. IEEE Int. Symp. Biomed. Imaging. 1142 (2009).
[15] J. Peng, Z. Du, Y. Piao, X. Yu, K. Huang, Y. Tang, P. Wei, and P. Wang, Front Hum Neurosci. **19**, 1536906 (2025).
[16] X. Su, J. Gua, M. Zhou, J. Chen, L. Li, Y. Chen, X. Sui, H. Li, and X. Chai, IEEE Trans. Neural. Syst. Rehabil. Eng. **29**, 418 (2021).
[17] C. Wolters and J. C. D. Munck, Scholarpedia. **2**, 1738 (2007).
[18] V. J. Bolfe, S. I. Ribas, M. Mil, and R. R. J. Guirro, Braz. J. Phys. Ther. **11**, 2 (2007).
[19] D. Miklavcic, N. Pavselj, and F. X. Hart, Electric Properties of Tissues, Wiley Encyclopedia of Biomedical Engineering (2006) pp. 1-12.
[20] H. McCann, G. Pisano, and L. Beltrachini, Brain Topogr. **32**, 825 (2019).
[21] S. B. Baumann, D. R. Wozny, S. K. Kelly, and F. M. Meno, IEEE Trans. Biomed. Eng. **44**, 220 (1997).
[22] I. Lackovic, R. Magjarevic, and D. Miklacvcic, World Congress on Medical Physics and Biomedical Engineering 210 (2009).
[23] J. Vorwerk, U. Aydin, C. H. Wolters, and C. R. Buston, Front Neurosci. **13**, 531 (2019).
[24] S. Pursiainen, F. Lucka, and C. H. Wolters, Phys. Med. Biol. **57**, 999 (2012).
[25] V. Tiruvadi, S. James, B. Howell, M. Obatusin, A. Crowell, P. R. Posse, R. E. Gross, C. C. Mclntyre, H. S. Mayberg, and R. Butera, IEEE Trans. Neural. Syst. Rehabil. Eng. **31**, 68 (2023).